Iraqi Journal of Oil & Gas Research, Vol. 04, No. 1 (2024)

Iraqi Journal of Oil & Gas Research

Journal homepage: https://ijogr.uotechnology.edu.iq/

Utilizing Kaolin-Based Geopolymer Catalysts for Improved Doura Vacuum Residue

[1] Tuqa A. Jabar1*, [1]Mohammed A. Alzuhairi, [1]Mayyadah S. Abed

[1]Material Engineering Department, University of Technology, Baghdad, Iraq.

Article information

Article history:
Received: December, 12, 2023
Accepted: March, 05, 2024
Available online: April, 08, 2024

Keywords:
Kaolin,
Geopolymer,
Catalyst,
Cracking,
Vacuum Residual (VR)

Corresponding Author:
Tuqa A. Jabar
mae.20.84@grad.uotechnology.edu.iq

Abstract

This study explores the viability of geopolymers as eco-friendly catalysts for cracking vacuum residuals (VR) into transportation fuels. Hierarchically porous geopolymers (G1 and G2) were synthesized with 60/40 red/white and white/red kaolin ratios, respectively. 2M HCl leaching was applied to increase surface area of G1 and G2 for enhanced adsorption and catalytic activity. Characterization via XRF, XRD, FTIR, BET, and GC-MS revealed: significant differences in Si/Al ratios and iron content (XRF), influencing cracking. Increased surface area (BET): 9.5-38.24 m²/g for G1 and 6-28.56 m²/g for G2 after acid treatment. Presence of acid sites and increased H+ (FTIR). Zeolite phase formation and increased crystallization after acid treatment (XRD).

Cracking performance: G1 achieved 86.52% total yield, with 33% gasoline (C5-C10) and 53.42% kerosene/jet fuel (C10-C16). G2 yielded 82.8%, with 23% gasoline and 59.74% kerosene/jet fuel. Both catalysts exhibited good cracking yields.

Catalyst comparison: The catalyst with higher Fe/SiO2-Al2O3 ratio (G1) showed superior efficiency in gasoline and kerosene production.

G2 demonstrated better sulfur removal from VR. Conclusions: Geopolymers offer potential as sustainable and affordable cracking catalysts. Further investigation is needed to optimize catalyst composition and reaction conditions.

DOI: http://doi.org/10.55699/ijogr.2024.0401.1061

1. Introduction

The Geopolymer is an inorganic polymer material made from constituents of the raw materials (aluminosilicate-source) and the activator in liquid form such as alkali or acid for activation reactions [1], [2], [3]. Geopolymer is created via an exothermic chemical reaction involving aluminosilicate and alkali [4]. The geopolymer, initially introduced by scientist Joseph Davidovits was discovered in 1972 as an environmentally friendly and innovative substitute for cement [5]. The geopolymers have three-dimensional frameworks consisting of silicon-oxygen tetrahedra and aluminum-oxygen tetrahedra that are connected alternately by sharing all oxygen atoms. Geopolymers possess an amorphous to semi-crystalline structure, contrasting the well-defined, crystalline nature of zeolites. While both share similar chemical compositions based on tetrahedral units of silicon and aluminum, the key distinction lies in their crystal structure. Geopolymers' variability stems from this amorphous nature, enabling tailored properties for specific applications, while zeolites' crystallinity offers uniform structures and defined pore sizes ideal for separation and adsorption processes [6].

The factors controlling the internal structure of geopolymers are the ratio of silicon to aluminum (Si/Al) and the types and quantity of activators used, the source and grading of aggregates, the duration and temperature of hardening/curing, the particle size, and heat treatment [7], [8]. Geopolymer foam structures possess ion exchange making them ideal for a new class of catalysis applications by increasing to active sit [9].

The petroleum industry (oil and gas) is very important and is considered the backbone of the Iraqi economy and the primary source of government revenue [10]. The crude oil is naturally liquid and has a mixture of complexes of hydrocarbons and non-hydrocarbons with different concentrations, which include impurity compounds of sulfur, oxygen, nitrogen, vanadium, copper, iron, nickel, sodium, zinc, and metals. Water is also found in petroleum [11], [12].

The vacuum residue is the lowest-value product from petroleum refining, which if not converted is mostly used for the production of road pavement bitumen and heavy fuel oil [13]. Vacuum residue (VR) can be defined as the heaviest distillation product or defined as carbon rejected from crude petroleum fraction through the refining process. VR has a low hydrogen to carbon (H/C) ratio, high viscosity (wax installation) with API gravity between 10 and 20°at room temperature, with black color VR including two fractions: extra heavy hydrocarbons and very high molecular weight like resins and asphalting. Vacuum residue was produced from the bottom of the vacuum distillation unit of the crude oil; however, crude oil origin yields 10–15% (VR). These VRs contain high impurities such as vanadium, nickel, calcium, iron, silica, compounds of oxygen, nitrogen, and sulfur. These VR can be classified into four organic fractions resins, aromatics, saturates, and asphaltenes [14]. In recent decades, researchers have emphasized the development of refining techniques based on cheaply available feedstocks, such as coal, grade petroleum oil, or wax [15],[16].

The catalyst's goals for the upgradation of heavy oils and VR are to decrease viscosity and boiling point, demetallation, desulfurization, level of other impurities, and increase the H/C ratio with high commercial values [17]. Cracking is defined as the process of breaking up large hydrocarbon molecules into small molecules. Catalysts are utilized to reduce pressures and temperatures [18], [19]. Cracking is one of the principal ways in which crude oil is converted into useful fuels such as motor gasoline, jet fuel, and home heating oil [20].

In (2022) K. S. AlKhafaji et al.'s study, they synthesized an economical catalyst using kaolin clay supported with alumina. The catalyst was compared with a conventional bi-functional catalyst in the Hydrodesulfurization (HDS) operation. Under specific conditions: a reaction temperature of 375°C, pressure at 40 bar, Liquid Hourly Space Velocity (LHSV) of 1 hr^{-1}, and an H_2/hydrocarbon (HC) ratio of 200 vol. ratio, the efficiency was determined to be 62.2%, with a substantial 90% hydrodesulfurization achieved [21]. L. Vieira et al.'s (2018) designed geopolymer from metakaolin for catalyst application with a high specific surface area. The ratio of Si/K was 2.46, and Si/Al was 1.37, resulting in an amorphous structure. The geopolymer exhibited a specific surface area of 75 m^2/g and a pores volume of 0.28 cm^3/g. The pores displayed a size distribution between 7 and 20 nm, resembling zeolites in terms of ion exchange and accommodation of metal ions. This suggests the geopolymer's potential for applications involving ion exchange and metal ion interactions similar to zeolitic materials [22].

This work aims to develop new catalysts made from geopolymers, to match the effectiveness of zeolites. The prepared geopolymer catalysts will be investigated in a fixed-bed reactor to see how well they convert oil into gasoline and other hydroarbones. Gas chromatography will be utilized to analyze the yield and composition of the resulting hyrocarbones, comparing it to standard gasoline. This comparison will help assess how efficient the geopolymer catalysts are at converting oil and the quality of the gasoline they produce.

2. Experimental work

2.1 Materials Used

The kaolin used in this work is a natural clay found in Iraq's Wadi Al-Sufi Anbar region, as the main raw material. Both alkaline solutions; Potassium hydroxide (KOH) and sodium silicate (Na_2SiO_3), were obtained from Thomas Baker Chemicals in Mumbai, India, to activate the material through a process called geopolymerization. Hydrogen peroxide (H_2O_2), a foaming agent, was supplied by Fine-Chem Ltd., India. Finally, hydrochloric acid (HCl), obtained from Thomas Baker Chemicals, India, was used to etch the geopolymer samples after they were formed.

2.2 Feed Used

The used heavy oil residue in this work was extracted from the Al-Doura petroleum refinery in Baghdad, Iraq, which displayed characteristics of a waxy texture, black color, and a composition rich in heavy hydrocarbons with elevated molecular weights. This specific residue, referred to as Doura Vacuum Residual (VR), is depicted in Figure 1.

Figure 1: Crud residue from Dura refinery.

2.3. Preparation for Pre-Geopolymerization

The kaolinite raw materials employed, both white and red variants, underwent chemical characterization through atomic absorption (AA240FS) and chemical analysis using xy-sampler chromatography following ASTM C 573 standards. Subsequently, the raw materials were crushed into a powder and sieved through a mesh with a ≤80μm aperture. Figure 2 illustrates the raw materials utilized in this process.

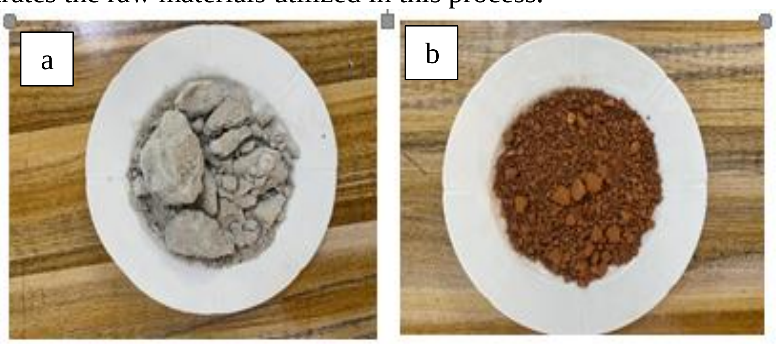

Figure 2: Kaolin used; a) White kaolin, and b) Red kaolin

The procedure entails transforming kaolin into metakaolin by subjecting it to electric furnace firing at 750°C for a duration of 2 hours. This process was carried out at the laboratories of the National Center for Construction in Baghdad [23]. Geopolymer preparation involves combining Metakaolin (MK) with varying percentages of red and white metakaolin, as outlined in Table 1. Alkaline substances, such as KOH (14M) and water glass

(Na2SiO3), were added in a 1:1 ratio to facilitate the formation of geopolymer precursors, with water glass serving a dual role by regulating the chemical composition and acting as a mineralizing agent [24].

The experimental process commenced by blending 15g of metakaolin in a glass cylinder using an electric blender for 15 minutes. Subsequently, a diluted hydrogen peroxide (H2O2) solution (1%) was introduced as a foaming agent to generate H2 and O2. Following an additional 30 minutes of continuous mixing, the mixture was poured into a plastic mold (1×1×2 cm3). After solidifying at room temperature for a day, the samples were cured in an oven at 100°C overnight. Figure 4 illustrates the various stages of geopolymer preparation. The schematic diagram for all the processes is shown in Fig 3.

Table 1: Mixing design of the prepared geopolymer

Type	Red Metakaolin %	White Metakaolin %
G1	60%	40%
G2	40%	60%

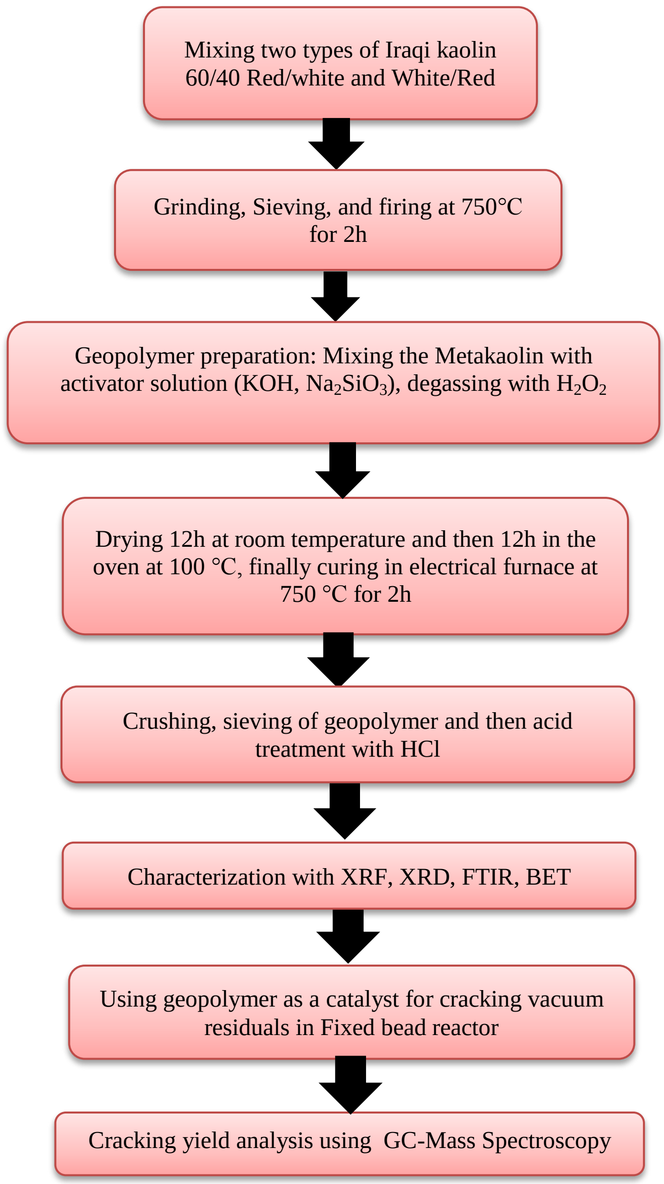

Figure 3: The schematic diagram of current work.

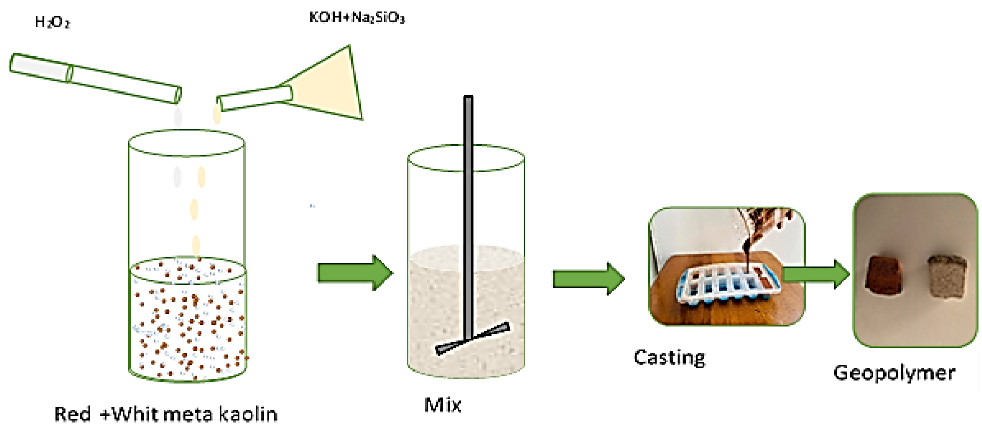

Figure 4: Geopolymer preparation procedure

2.4. Acidic treatment

The obtained geopolymer was finely ground into a powder and then treated with HCl (2M) to gain G1* and G2*. This acid treatment lasted for 48 hours, after which the geopolymer underwent extensive rinsing with distilled water and was left to dry at room temperature overnight. Subsequently, the dried geopolymer was subjected to firing at 750°C for a duration of 2 hours. The step-by-step process of catalyst preparation is depicted in Figure 5 [25], [26]. The geopolymer catalysts, notably, undergo a post-treatment involving dealumination and desilication using HCl. This process serves to increase the surface area and improve the distribution of electronic charge among the active sites [27].

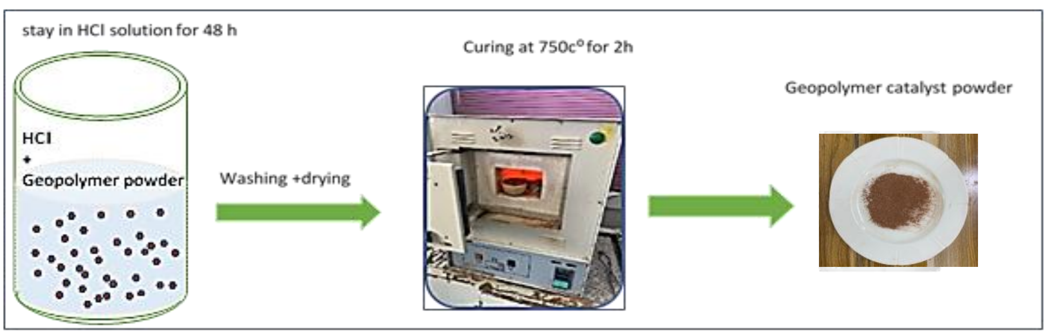

Figure 5: Catalyst preparation procedure

2.5. Cracking Unit

This experiment uses a custom-built reactor (shown in Figure 6) to convert heavy residue from the Doura Refinery into lighter, more valuable products. This process is important because it takes thick, unusable oil and makes it more useful.

The reactor is like a metal tube (stainless steel) with a heater to control the temperature. It has valves, a pressure gauge, and a thermometer inside to carefully watch what's happening during the experiment. The key part is the geopolymer, which sits in the middle, packed tightly inside a small metal container to work best. The reactor is wrapped in glass wool to keep the heat in, and a plastic tube connects the container to a glass system where the finished product collects. The pressure gauge at the reactor's top monitors pressure conditions throughout the cracking process. VR is introduced into the reactor, and as internal temperature rises, heavy oil molecules reach boiling points, ascending within the cylinder and entering the catalyst tube containing geopolymer. The cracking process occurs, yielding smaller hydrocarbon molecules.

Real-time temperature monitoring and control are facilitated by the internal sensor during cracking, producing valuable products like gasoline and diesel fuel. After completion, the condensed products are collected through the glass system for separation based on boiling points.
In summary, this reactor configuration proves efficient for VR cracking, converting heavy crude oil into valuable products. Temperature and pressure monitoring devices ensure optimal conditions, and insulation materials contribute to process efficiency.

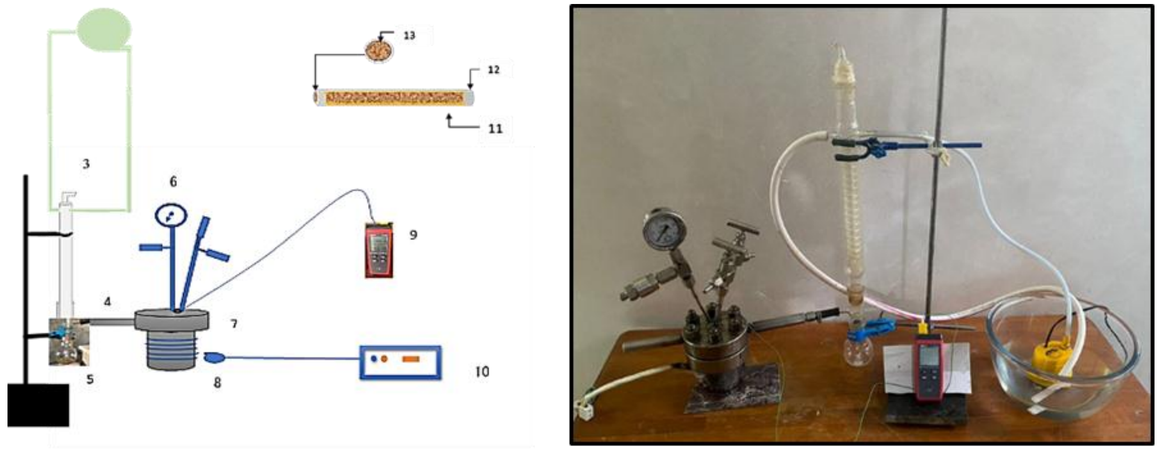

Figure 6: Fixed bed reactor device consisting of 1- Water pump, 2- Coldwater, 3- Condenser, 4- Fixed bed, 5- Collect liq. ,6- gauge pressure, 7- Autoclave, 8- Heater, 9- Thermocouple, 10- Power supply, 11- Fiberglass, 12- Bed reactor, 13- Geopolymer catalysts.

3. Characterization of the Geopolymer

Comprehensive characterization of geopolymer samples involved multiple techniques, including XRD, XRF, BET, and FTIR. Phase identification through X-ray diffraction employed the Shimadzu XRD 600 model with analytical software. Chemical composition analysis utilized the XRF Spectrometer (XEPOS spectrometer, SPECTRO XEPOS spectrometer, Analytical instruments 4 kW /PW100) with a Rh X-ray tube. Time-gated FTIR spectroscopy was applied to geopolymer samples both before and after treatment with HCl.
Specific surface areas and pore volumes were determined using the Micromeritics ASAP 2020 device via nitrogen physisorption at -196°C. The BET method calculated surface areas, and samples were vacuum degassed at 100°C for 1200 minutes prior to adsorption. The analysis exhibited an inaccuracy of ±5 m²/g.

4. Results and Discussion

4.1 Chemical analysis of kaolin

Table 2 presents the chemical composition of the kaolin utilized in this study. The analysis reveals the primary components as alumina, silica, and iron oxide. Both white and red kaolin exhibit a silica content approximately twice that of alumina. Specifically, white kaolin has a silica content exceeding red kaolin by approximately 12%. However, red kaolin is enriched with a higher concentration of iron oxide compared to white kaolin.

Table 2: Chemical analysis of Iraqi local kaolin.

Type	**SiO_2%**	**Al_2O_3%**	**Fe_2O_3%**	**Rest%**
White kaolin	54.00	28	3.40	15%
Red kaolin	43.22	22	15.92	19%

Table 3 outlines the results of XRF analysis for the geopolymer before HCl treatment, while Table 4 displays the outcomes after treatment. The Si/Al ratio undergoes noticeable changes, especially post HCl treatment, indicating induced dealumination of aluminum during the process. G1 exhibits different behavior compared to G2 under HCl treatment. Additionally, a decrease in iron content is observed, impacting both mechanical and chemical characteristics. In Table 4, after treatment with 2M HCl, G2 experiences significant dealumination and desilication, while G1 sees the removal of iron oxide, resulting in a clear impact on the overall Si/Al ratio. This reduction in iron content influences both the internal structure and chemical activity. G1, in particular, shows a substantial reduction in iron and an impact on achieving a higher Si/Al ratio. Summarizing the leaching experiments, the resistance of geopolymers to acidic attack strongly depends on the Si/Al ratio. Structural differences among geopolymers were confirmed to influence stability against acidic attack [28]. The minor rise in the concentration of certain elements is attributed to their high resistance to acid, while the overall mass experiences a decrease in the presence of acid.

Table 3: XRF for geopolymers before treatment

Geopolymer	Si%	Al%	Fe%	K%	Na%	Ca%	Ti%	Rest %
G1	39.8	4.25	44.85	1.8	1.5	0.8	6.18	0.9
G2	31.2	6.78	16.5	36.36	2	6.2	2	0.7

Table 4: XRF for geopolymers after HCl treatment

Geopolymer	Si%	Al%	Fe%	K%	Na%	Ca%	Ti%	Rest%
G1	54.5	6.07	25.99	2.4	2.3	0.8	7.6	1.33
G2	23.65	4.14	31.17	28.15	1.3	8.91	2.1	0.58

4.2 X-Ray Diffraction

XRD analysis confirmed the amorphous nature of the geopolymer, as expected [29]. However, examination of samples with different mixing ratios (Figures 7 and 8) revealed some unexpected crystalline phases.

Using "X'Pert High Score Plus", the following observations were made: Sample G1 (Figure 7) exhibited a broad hump at 26.4° 2θ, indicative of a zeolite-like phase (reference code 01-083-2369), specifically a cubic phase with peaks at 10.03°, 20.6°, 26.39°, 49.9°, 59.8°, and 67.89° 2θ. Minor phases of quartz (SiO2), mullite (3Al2O3 2SiO2 or 2Al2O3SiO2), and hematite (Fe2O3) were also detected [30], [31]. X-ray diffraction (XRD) analysis of the 60% red geopolymer treated with acid (G1) revealed the presence of a zeolite-like phase according to reference code (01-083-2369). This phase exhibits a cubic structure with peaks at 10.02°, 16.535°, 20.3°, 26.37°, 32.9°, 36.3°, 39.42°, 45.5°, 49.7°, 59.38°, 59.6°, 62.3°, 63.8°, 67.7°, and 75.3° 2θ.

An additional minor cubic phase identified as Zeolite X, syn, according to reference code (01-071-1012), was also detected with a peak at 13.3° 2θ.

Furthermore, the XRD analysis revealed an increase in crystallinity of the geopolymer after acid treatment. The degree of crystallinity increased from 19.9% for the untreated G1 sample to 35.19% for the sample treated with acid (G1*).

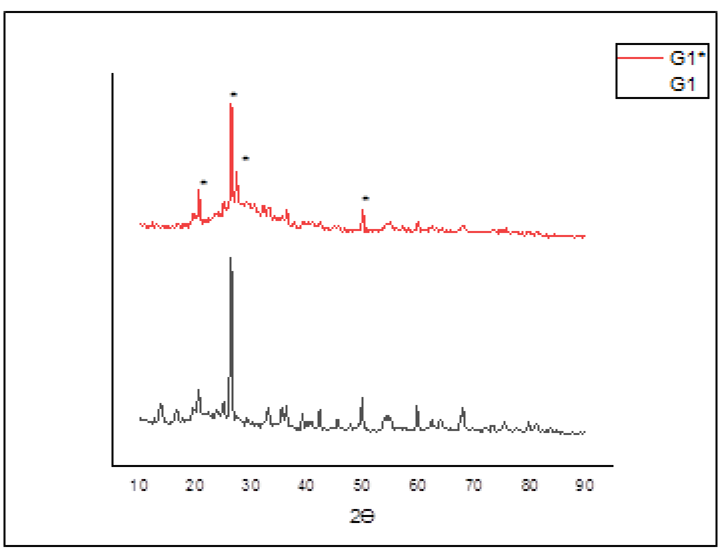

Figure7: XRD Patterns of G1 and G1*

XRD analysis of the 60% white kaolin geopolymer (G2) identified a cubic zeolite-like phase according to reference code (01-083-2369) (Figure 8). This phase displayed peaks at 2θ values of 20.7°, 24.26°, 26.33°, 39.35°, 41.49°, 54.3°, 60°, 64.3°, 68.2°, and 72.2°. Interestingly, XRD analysis of the acid-treated 60% white kaolin geopolymer (G2) revealed the same* major cubic zeolite-like phase (reference code 01-083-2369), but with additional peaks at 2θ values of 33.39°, 35.8°, 49.9°, 75.4°, 79.8°, and 81.2° (Figure 8). This suggests that acid treatment promoted the formation of a more crystalline zeolite-like phase in G2*.
Furthermore, XRD analysis indicated an increase in the degree of crystallinity for both geopolymers after acid treatment. The crystallinity increased from 23.9% for the untreated G2 sample to 35.8% for the acid-treated G2* sample. This observation aligns with the presence of additional peaks in the XRD pattern of G2*.

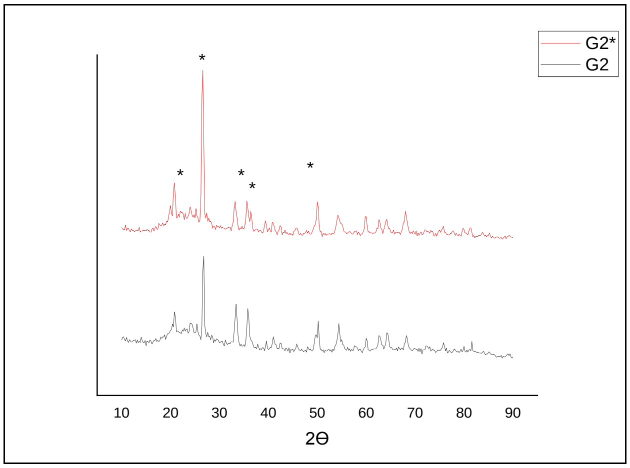

Figure 8: XRD Patterns of G2 and G2*

Acid treatment of geopolymer (G1 & G2) to be (G1* & G2*) resulted in a shift in the amorphous hump in the XRD patterns towards lower angles. This shift reveals the formation of a new, potentially amorphous phase [32]. However, the degree of crystallinity remained relatively low, indicating the limited conversion of the geopolymer into zeolite phases [33].
In spite of the low crystallinity, research [33] found the presence of crystalline structures and several zeolite types within the modified geopolymers. This suggests that the acid treatment may have accelerated the condensation of free Si-OH groups during the hydrothermal process, partially transforming the geopolymer into zeolite-like structures. Additional studies by Zhang et al. [34], provide further evidence for this mechanism.

4.3 Fourier Transform Infrared Spectroscopy FTIR analyses
the functional groups present in geopolymers was investigated by FTIR analysis. The samples were synthesized from varying red and white kaolin types. Samples were prepared as KBr pellets and scanned in the 4000-450 cm-1 range. The focus was to identify changes in chemical structure by tracking key functional groups in the IR spectra.
All specimens revealed characteristic bands of aluminosilicate materials, indicating the presence of Al-O, Si-O, and other related bonds (Figures 9 and 10). Specifically: G1 and G2 spectra showcased a broad band at 1054 cm-1, attributed to the asymmetric stretching of Si-O-Si bonds. A band at 796-850 cm-1 corresponded to the bending of Si-O-Si bonds [35], [36], [37]. The main peak at 1052 cm-1 suggested Si-O-Si and/or Si-O-Al bonds, while the peak around 780 cm-1 indicated Al-O vibrations in Al_2O_3 structures [38].
The band at 870 cm-1 potentially pointed to Al-O symmetric stretching in tetrahedral coordination, further supporting geopolymer formation.
Additional peaks at 1085 cm-1 confirmed Si-O-Si stretching and O-Si-O bending modes, while peaks at 3445 and 1634 cm-1 suggested the presence of water and silanol groups based on cited literature. Notably, these peaks were sharper and more intense due to changes in chemical composition and increased acidity. Bands at 3406, 1652, 1541, and 1459 cm-1 corresponded to OH stretching vibrations and H-O-H bonds of free water [39], [40].
In conclusion, FTIR analysis confirmed the presence of geopolymers and provided insights into their specific functional groups. The observed changes in peak intensities and locations suggest altered chemical composition and increased acidity upon modification.

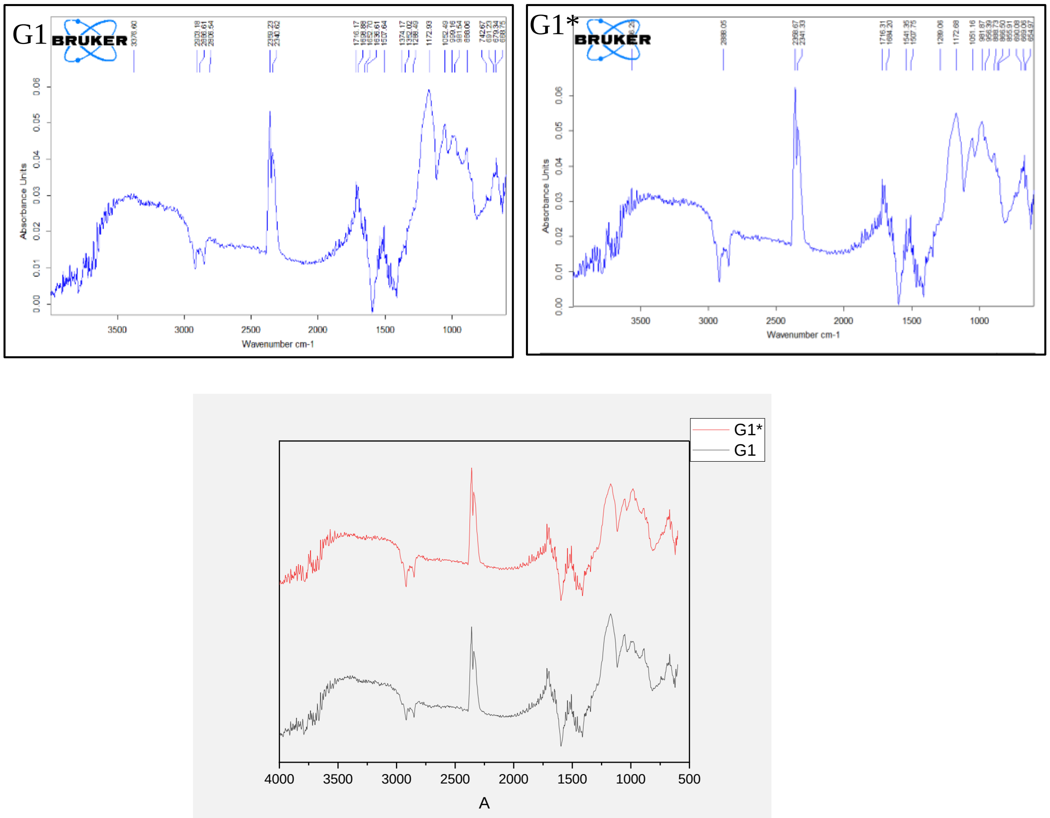

Figure 9: FTIR of geopolymer G1, G1* (without treatment, and after treatment).

The G2 spectrum exhibits a broad band in the 950-615 cm⁻¹ range, while G2 shows a narrower band ranging from 888-653 cm⁻¹. Both spectra present a peak at 1054 cm⁻¹ shifted to 1060 cm⁻¹ in G2*, suggesting a change in the Si/Al ratio due to dealumination caused by acid treatment. These bands are typically attributed to the asymmetric stretching of Si-O-Si and/or Si-O-Al bonds.

Additionally, the G2 spectrum displays a broader band encompassing Si-O-Si bending and Al-O vibrations in Al2O3 structures (950-653 cm⁻¹) compared to G2 (888-653 cm⁻¹). This further supports the notion of altered Si/Al composition due to acid treatment. Notably, several peaks become sharper and exhibit increased intensity in both spectra, likely reflecting changes in chemical composition and increased acidity [36], [37], [38].

Both G2 and G2* spectra showcase bands at 3566, 1716, 1541, and 1457 cm⁻¹, which can be assigned to OH stretching vibrations and H-O-H bonds associated with free water [40],[41]. Furthermore, the band at 3641 cm⁻¹ in both spectra could be attributed to H-bonded vicinal silanols and bridging hydroxyls (Brønsted OH) according to reference [32].

In summary, the FTIR analysis reveals distinctive differences between G2 and G2 spectra, indicating changes in the Si/Al ratio and functional groups induced by acid treatment. The observed peak shifts, band narrowing, and intensity variations provide valuable insights into the structural modifications experienced by the geopolymer upon acid treatment.

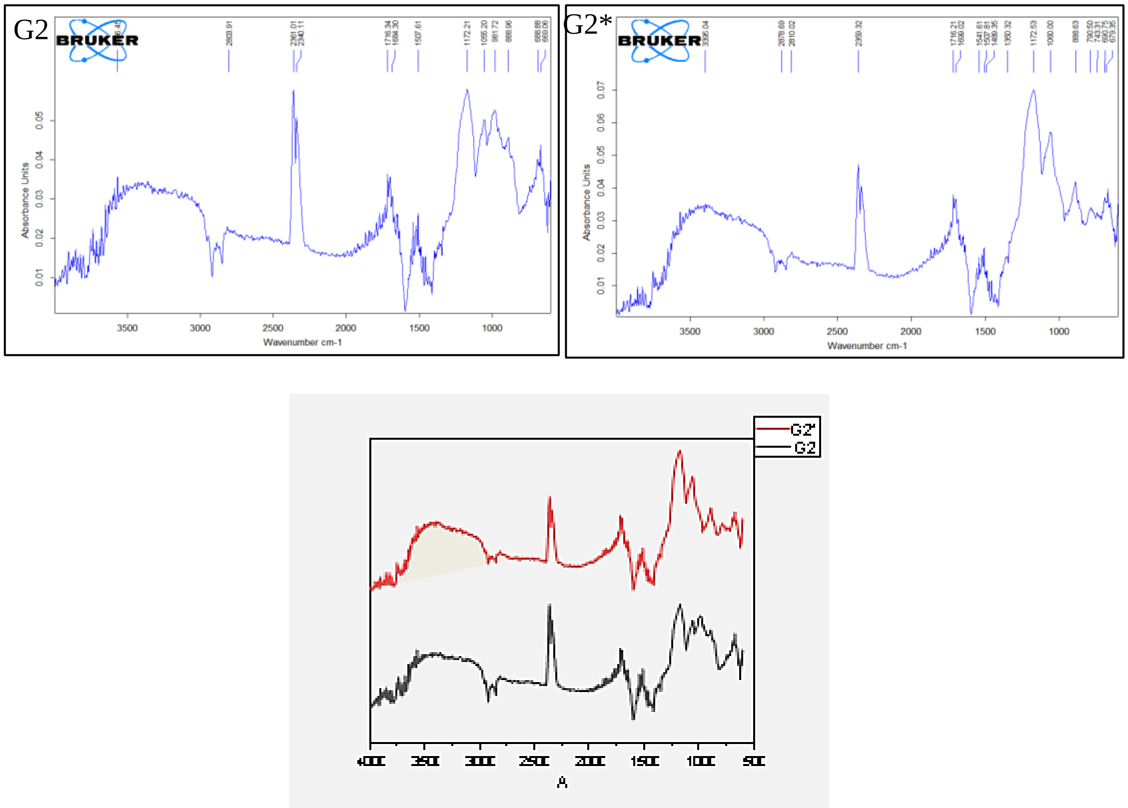

Figure 10: FTIR of geopolymer G2, and G2*

FTIR analysis complemented the XRD results, and observed peaks were assigned to specific bands: 460 cm-1 (Si-O-Si and O-Si-O bonds). The number of acid sites in geopolymers has been found by FTIR spectroscopy to increase in all geopolymers (G1, G1*, G2, G2*).

However, the Acidity of zeolite significantly depends on the Si/Al ratio, and in this case, if the Si is in the zeolite framework, how it will affect the acidity and catalytic activity?

After treatment the Si/Al ratio increases, and the total molar ratios of Al IV and Al V increase, which affects the Brønsted acid site density in the geopolymer [36], [38]. The metastable aluminum (AlIV and AlV) aluminum atoms are incorporated into the proximity to silanol groups, this local structure of the silanol groups close to aluminum behaves as a “pseudo-bridging silanol” model, these metastable aluminum (AlIV and AlV) atoms could induce an electron density transfer from neighboring silanol groups, which can enhance the acid strength of neighboring silanol groups and to form Brønsted acid sites which aligns with the previous studies [42]. That is, there is a correlation between the total Al IV-Al V molar composition and the total Brønsted acidic sites density Brønsted and Lewis acid sites samples were discriminated by FT-IR from peaks at 1540 and 1450 cm−1, which aligns with the findings of previous studies [43], [44], [45]. Also 1445 cm-1 (Lewis acid sites), 1547 cm-1 (Brønsted acid sites) at 1490 cm-1 [46].

Also, three principal vibrational bands at 2307–2311, 2272, and 2261 cm−1, were assigned to adsorption on Lewis and Brønsted acid sites. This characterization suggests that the Brønsted acidity increases through the introduction of OH groups on the metallic nodes during the hydrothermal synthesis [47], [48].

4.4 Brunauer Emmett Teller BET analyses

The surface area of the geopolymers prepared in this study was determined using the Brunauer Emmett Teller (BET) method. Notably, there was a substantial change in surface area after acid treatment, and this change varied according to the Si/Al ratio, as illustrated in the BET results prove the large effect of HCl on the surface geopolymers leaching that clear in the Figure 11 the Initial value of surface area was, G1 and G2 demonstrated

surface areas of 9.5 and 6 m²/g, respectively. However, after treatment, the surface areas increased to 38.24 and 28.56 m²/g, as and these increase vary with iron content (iron large effect with acid)[49].
The pore volume of G1 increased after treatment, as depicted in Figure 12, revealing the significant effect of iron content on the range of HCl treatment. In contrast, the pore volume showed a different effect with G2. Specifically, these results suggest that minor variations in surface area were observed with different catalyst mixtures. However, upon acid treatment, the samples exhibited a substantial increase in BET surface areas, particularly with increased iron content compared to previous reports. The HCl leaching caused an exchange of Al3+, Fe3+, and Mg2+ with H+ ions, leading to a surface area increase of more than four times the activated state [41]. Indeed, the use of acid treatment, such as HCl, on zeolite typically results in the removal of aluminum, a process known as dealumination. This dealumination process is employed to introduce porosity into zeolites, thereby modifying their structure and properties [50].
The observed increase in specific surface area can be attributed to significant dealumination within the geopolymer. Conversely, the increase in the Si/Al ratio, consistent with XRF results, resulting from aluminum leaching, led to enhanced porosity and specific surface area in the samples. Furthermore, acid leaching influenced pore size distribution, primarily enhancing mesoporous characteristics in the geopolymers [51]. Importantly, the impact of acid leaching on specific surface area and pore size distribution was more pronounced than that induced by calcination.

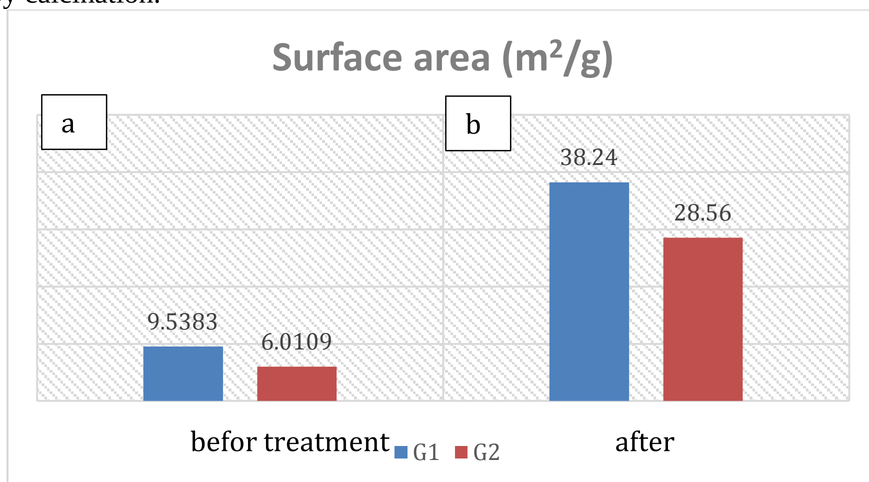

Figure 11: surface area of geopolymer G1, and G2
a) before treatment, b) after treatment.

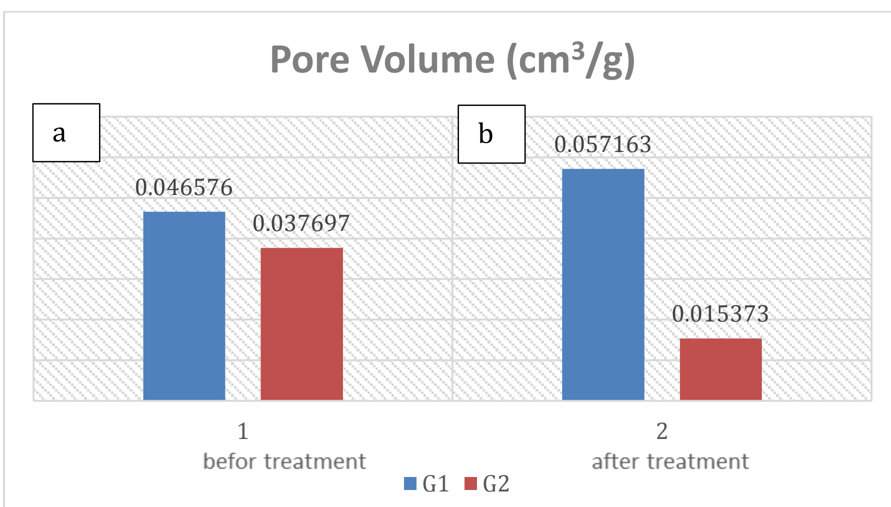

Figure 12: pore volume of geopolymer G1and G2
a) Before treatment, b) after treatment

4.5 Gas chromatography-mass spectrometry (GC–MS).

Gas chromatography-mass spectrometry (GC-MS) is employed in this study for the quantification and identification of individual components within oil samples. The AGILENT 7890A GC and AGILENT 5975C MS operating in EI mode with a Mass Spectrometer detector are utilized. The Mass Spectrometer scan range is set at 50-500, with an electron energy (EM) of 70 eV and a temperature of 260°C.

GC-MS is used to analyze the final liquid products derived from Vacuum Residual (VR) using various Geopolymer catalyst types. The products are categorized into fractions based on the number of carbon atoms to assess the Geopolymer catalysts' performance comprehensively.

The chemical composition of Doura Vacuum Residual (VR) determined by GC-MS is presented in Table 5 encompassing a range from C12 to C32. These components, consisting of heavy hydrocarbons with high molecular weights, are transformed into more viable products through the cracking process facilitated by the cost-effective Geopolymer catalyst.

The liquid products obtained from the G1, G1*, G2, and G2* catalysts are detailed in tables 6,7,8,9 displaying a wide carbon range (C5-C24). Notably, Dodecane ($C_{12}H_{26}$) is observed at a high concentration, with a value of 4.01. This compound is influenced by the active Fe_2O_3 species present in the original red kaolin [42]. The G1 geopolymer catalyst yields 33% for gasoline (C5-C10) and 53.42% for kerosene and jet fuel (C10-C16) products, showcasing its novel role as a catalyst. Similarly, the G2 catalyst produces liquid products with a broad carbon range (C8-C24), with 1-Tridecene ($C_{13}H_{26}$) as a prominent compound, reaching a concentration of 6.52 catalytically. Notably, the G2 catalyst yields a higher quantity of gasoline (C5-C10) at 23% and kerosene and jet fuel (C10-C16) at 59.74%. Figures 16 illustrate the compounds identified. The figure 13 shows oil yield from cracking prosses light oil have (gasoline, deasil, kerosine) the carbons rang was from (C5-C16) for use geopolymers catalysts G1, G1*, G2, and G2*. The highest yield was G1* (60% red and 40 white kaolin treated with HCl). This result due to Si/Al ratio, high degree of crystallinity and Zeolite phase in all this factor gives it good performance through cracking process.

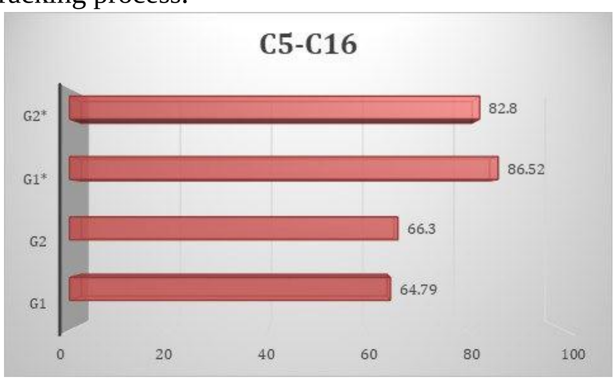

Figure 13: VR cracking yield by geopolymer catalyst

Table 5: The compounds identified through Gas Chromatography-Mass Spectrometry (GC-MS) analysis of Vacuum Residual (VR) from Doura Refinery

GCM for vacuum residual (VR)					
No	RT (min)	Area (Ab*s)	Hit Name	Quality	CAS Number
1	19.7	18466253	Diethyl Phthalate	98	000084-66-2
2	20.654	2459452	Hexadecane	93	000544-76-3
3	21.521	1933820	Amiphenazole	38	000490-55-1
4	22.507	1222952	Heptadecane	76	000629-78-7
5	24.701	4347949	Phthalic acid, hexyl octadecyl ester	72	1000309-06-2

Table 6: The compounds identified through Gas Chromatography-Mass Spectrometry (GC-MS) analysis of used G1

No	RT (min)	Area%	Name	Quality	CAS Number
1	4.211	0.28	Cyclopropane, pentyl-	52	002511-91-3
2	4.378	0.80	p-Xylene	83	000106-42-3
3	4.507	0.42	Octane, 4-methyl-	49	002216-34-4
4	4.652	0.69	Octane, 3-methyl-	58	002216-33-3
5	4.964	1.09	1-Nonene	81	000124-11-8
6	5.213	1.51	Nonane	91	000111-84-2
7	6.38	0.29	trans-3-Decene	64	019150-21-1
8	6.619	0.65	Heptane, 2,3,4-trimethyl-	47	052896-95-4
9	6.764	0.39	Heptane, 5-ethyl-2,2,3-trimethyl-	50	062199-06-8
10	6.956	0.20	Mesitylene	95	000108-67-8
11	7.164	0.99	1-Decene	96	000872-05-9
12	7.309	0.24	Cyclohexane, 1,2,3-trimethyl-, (1.alpha.,2.beta.,3.alpha.)-	64	001678-81-5
13	7.475	1.76	Decane	91	000124-18-5
14	7.61	0.35	Mesitylene	95	000108-67-8
15	7.74	0.25	Heptane, 3,3-dimethyl-	38	004032-86-4
16	7.833	0.23	Benzene, 2-propenyl-	53	000300-57-2
17	8.004	0.38	Decane, 4-methyl-	90	002847-72-5
18	8.238	0.24	Cyclopentane, hexyl-	60	004457-00-5
19	8.497	0.24	cis-3-Decene	49	019398-86-8
20	8.684	0.23	Benzene, 1-methyl-4-propyl-	35	001074-55-1
21	8.98	0.30	o-Cymene	91	000527-84-4
22	9.13	0.67	Benzene, 4-ethyl-1,2-dimethyl-	60	000934-80-5
23	9.26	0.27	8-Oxabicyclo[5.1.0]oct-5-en-2-ol, 1,4,4-trimethyl-	50	058795-43-0
24	9.416	0.37	1-Nonene	70	000124-11-8
25	9.587	1.73	Cyclopropane, 1-heptyl-2-methyl-	91	074663-91-5
26	9.909	2.39	Undecane	90	001120-21-4
27	10.578	0.79	Benzene, 2-ethenyl-1,4-dimethyl-	92	002039-89-6
28	10.734	1.75	Benzene, 1,2,4,5-tetramethyl-	95	000095-93-2
29	10.894	0.27	2-Acetonylcyclohexanone	42	006126-53-0
30	11.107	0.22	Cyclopentane, 1-methyl-2-(4-methylpentyl)-, trans-	25	066553-50-2
31	11.304	0.47	Undecane, 4-methyl-	76	002980-69-0
32	11.413	0.43	Undecane, 2-methyl-	64	007045-71-8
33	11.559	1.03	2-Butene, 3-chloro-1-phenyl-, (Z)-	74	016608-68-7
34	11.751	0.48	1H-Indene, 2,3-dihydro-1,2-dimethyl-	83	017057-82-8
35	11.834	0.30	2-Undecene, 10-methyl-	46	1000061-83-3
36	12.01	1.32	2-Dodecene, (E)-	93	007206-13-5
37	12.093	0.32	Cyclopentane, (2-methylpropyl)-	45	003788-32-7
38	12.311	2.79	Dodecane	95	000112-40-3
39	12.518	0.26	Cyclododecane	64	000294-62-2
40	12.633	1.00	Undecane, 2,6-dimethyl-	93	017301-23-4
41	12.778	0.40	1H-Indene, 2,3-dihydro-1,1,3-trimethyl-	72	002613-76-5
42	13.292	0.61	Benzene, 1-methyl-3-(1-methyl-2-propenyl)-	41	052161-57-6
43	13.51	0.64	Decyl octyl ether	58	1000406-38-3

44	13.66	0.50	Dodecane, 2-methyl-	42	001560-97-0
45	13.904	0.58	1-Iodo-2-methylundecane	72	073105-67-6
46	13.997	0.23	Sulfurous acid, 2-ethylhexyl heptadecyl ester	49	1000309-20-0
47	14.117	1.22	Benzo[b]thiophene, 2-methyl-	87	001195-14-8
48	14.21	0.21	Benzene, 1-(2-butenyl)-2,3-dimethyl-	35	054340-85-1
49	14.335	1.22	1-Tridecene	98	002437-56-1
50	14.433	0.64	3-Tetradecene, (E)-	93	041446-68-8
51	14.625	2.88	Tridecane	95	000629-50-5
52	14.999	0.44	Carbonic acid, prop-1-en-2-yl tridecyl ester	80	1000382-90-8
53	15.16	0.25	Benzaldehyde, 4-methyl-	25	000104-87-0
54	15.761	0.71	Carbonic acid, decyl undecyl ester	30	1000383-16-0
55	15.896	0.60	Dodecane, 4-methyl-	38	006117-97-1
56	16.016	0.54	Benzene, 1,3,5-triethyl-	64	000102-25-0
57	16.145	0.24	3,5-Dimethyldodecane	60	107770-99-0
58	16.27	0.27	2,5-Dimethylthiophene-3,4-dicarbonitrile	83	1000305-40-9
59	16.467	0.89	Benzo[b]thiophene, 3,5-dimethyl-	97	001964-45-0
60	16.545	0.91	2-Tetradecene, (E)-	98	035953-54-9
61	16.825	3.04	Tetradecane	96	000629-59-4
62	16.898	0.21	Decane, 3,8-dimethyl-	55	017312-55-9
63	17.012	0.50	Pentadecafluorooctanoic acid, tetradecyl ester	43	1000406-04-4
64	17.458	0.42	4,4-Dimethyladamantan-2-ol	56	1000210-61-2
65	17.707	0.32	Cyclotetradecane	93	000295-17-0
66	17.795	0.48	Carbonic acid, dodecyl vinyl ester	46	1000382-54-8
67	17.93	0.37	1-Decanol, 2-hexyl-	50	002425-77-6
68	18.013	0.43	Tetradecane, 4-methyl-	80	025117-24-2
69	18.133	0.39	Decane, 3,6-dimethyl-	60	017312-53-7
70	18.252	0.28	Tetradecane, 3-methyl-	89	018435-22-8
71	18.475	3.00	Benzo[b]thiophene, 2-ethyl-5-methyl-	91	016587-51-2
72	18.641	0.52	2-Tetradecene, (E)-	97	035953-54-9
73	18.719	1.29	2,4-Pentanedione, 3-phenyl-	64	005910-25-8
74	18.895	2.59	Pentadecane	96	000629-62-9
75	19.061	0.63	Benzo[b]thiophene, 2,5,7-trimethyl-	76	016587-65-8
76	19.264	0.23	Naphthalene, 2,3,6-trimethyl-	66	000829-26-5
77	19.404	0.44	1,4-Cyclohexadiene, 6-isopropenyl-1,2,3,4-tetramethyl-	70	1000160-89-3
78	19.58	0.79	Benzo[b]thiophene, 2,7-diethyl-	70	016587-45-4
79	19.798	0.34	Cyclopentadecane	90	000295-48-7
80	19.892	0.57	4,5,6,7-Tetramethylphthalide	49	029002-54-8
81	20.011	1.07	Benzo[b]thiophene, 2,7-diethyl-	89	016587-45-4
82	20.104	0.27	Pentadecane, 2-methyl-	66	001560-93-6
83	20.234	0.58	Pentadecane, 3-methyl-	68	002882-96-4
84	20.333	0.24	Benzo[b]thiophene, 2,3-diethyl-	90	054789-20-7
85	20.436	0.35	Benzene, 1-ethyl-3,5-diisopropyl-	64	015181-13-2
86	20.587	0.90	Cetene	93	000629-73-2
87	20.685	0.38	Benzo[b]thiophene, 2,3-diethyl-	70	054789-20-7
88	20.851	2.55	Hexadecane	97	000544-76-3
89	21.505	0.28	Benzo[b]thiophene, 2-ethyl-5,7-dimethyl-	70	018428-05-2

90	21.671	0.31	Tetradecane, 1-chloro-	42	002425-54-9
91	21.791	0.73	Decane, 3,6-dimethyl-	83	017312-53-7
92	21.998	1.12	Hexadecane, 2-methyl-	56	001560-92-5
93	22.128	0.56	Tetradecane, 1-chloro-	62	002425-54-9
94	22.361	0.26	4-(2,6,6-Trimethyl-cyclohexa-1,3-dienyl)-pent-3-en-2-one	66	1000192-39-9
95	22.47	0.65	3-Heptadecene, (Z)-	97	1000141-67-3
96	22.704	2.28	Heptadecane	96	000629-78-7
97	22.828	0.24	Heptadecane, 3-methyl-	78	006418-44-6
98	23.181	0.26	Cyclotetradecane	60	000295-17-0
99	23.908	0.67	Heptadecane, 3-methyl-	95	006418-44-6
100	24.245	0.63	1-Octadecene	99	000112-88-9
101	24.463	2.04	Octadecane	97	000593-45-3
102	25.023	0.45	1-Methyldibenzothiophene	91	031317-07-4
103	25.142	0.34	Hexadecane, 1-chloro-	50	004860-03-1
104	25.386	0.57	2-Methyldibenzothiophene	72	1000383-55-1
105	25.49	0.30	Anthracene, 1-methyl-	89	000610-48-0
106	25.62	0.29	Octadecane, 3-methyl-	90	006561-44-0
107	25.926	0.30	1-Octadecene	99	000112-88-9
108	26.139	1.71	Nonadecane	97	000629-92-5
109	26.408	0.41	Dibenzothiophene, 4,6-dimethyl-	98	001207-12-1
110	26.761	0.66	3,7-Dimethyldibenzothiophene	98	001136-85-2
111	27.125	1.15	3,7-Dimethyldibenzothiophene	96	001136-85-2
112	27.737	1.62	Eicosane	99	000112-95-8
113	27.841	0.33	Phenanthrene, 3,6-dimethyl-	60	001576-67-6
114	28.302	0.26	4'-Methoxy-2-hydroxystilbene	55	1000147-93-1
115	28.432	0.29	(Acridin-9-yl)(methyl)amine	30	1000305-13-9
116	28.583	0.34	Benzenamine, 4,4'-methylenebis[2-methyl-	64	000838-88-0
117	28.676	0.21	1-Octadecene	91	000112-88-9
118	28.754	0.36	Anthracene, 1,8-diethynyl-	86	078053-58-4
119	28.941	0.36	5(10H)-Pyrido[3,4-b]quinolone, 7-methoxy-	83	1000256-99-5
120	29.252	1.78	Heneicosane	98	000629-94-7
121	29.797	0.20	Hexadecane	95	000544-76-3
122	29.973	0.38	[2,2'-Bithiophene]-5,5'-dicarboxaldehyde	64	1000327-35-6
123	30.71	1.23	Heptadecane	98	000629-78-7
124	31.249	0.20	1-Chloroeicosane	95	042217-02-7
125	32.106	1.25	Octadecane	96	000593-45-3
126	33.449	0.97	Tetracosane	98	000646-31-1
127	33.942	0.36	5-Methylbenzo[b]naphtho[2,1-d]thiophene	91	004567-49-1
128	34.233	0.32	3-Methylphenanthro[9,10-b]thiophene	89	082420-70-0
129	34.601	0.29	2,6,10,14-Tetramethyl-7-(3-methylpent-4-enylidene) pentadecane	93	1000370-41-6
130	34.736	0.88	Octadecane	97	000593-45-3
131	35.157	0.29	1-Chloroeicosane	95	042217-02-7
132	35.976	0.75	Triacontane	98	000638-68-6
133	36.189	0.21	1-Hexacosene	93	018835-33-1
134	36.376	0.23	Docosane	93	000629-97-0
135	36.718	0.20	Eicosane	95	000112-95-8
136	37.17	0.55	Eicosane	98	000112-95-8

137	37.398	0.48	1,4-Benzenedicarboxylic acid, bis(2-ethylhexyl) ester	91	006422-86-2
138	38.322	0.47	Octacosane	98	000630-02-4
139	39.437	0.50	Heptacosane, 1-chloro-	98	062016-79-9
140	40.516	0.40	Triacontane	98	000638-68-6
141	41.684	0.33	Heptacosane, 1-chloro-	99	062016-79-9
142	43.028	0.29	Heptacosane, 1-chloro-	98	062016-79-9
143	44.6	0.21	Tritriacontane	98	000630-05-7
144	46.478	0.26	Nonacosane	99	000630-03-5
145	48.72	0.22	Tritriacontane	97	000630-05-7

Table 7: The compounds identified through Gas Chromatography-Mass Spectrometry (GC-MS) analysis of used G1***.**

No	RT (min)	Area%	Name	Quality	CAS Number
1	4.377	0.91	Benzene, 1,3-dimethyl-	86	000108-38-3
2	4.502	0.82	Octane, 4-methyl-	46	002216-34-4
3	4.647	0.73	Octane, 3-methyl-	72	002216-33-3
4	4.782	0.31	p-Xylene	95	000106-42-3
5	4.959	1.07	1-Nonene	81	000124-11-8
6	5.218	2.19	Nonane	91	000111-84-2
7	5.617	0.20	Ethylidenecycloheptane	87	010494-87-8
8	5.752	0.24	Decane, 4-cyclohexyl-	50	013151-75-2
9	5.934	0.31	Octane, 2,6-dimethyl-	87	002051-30-1
10	6.095	0.27	Heptane, 3-ethyl-2-methyl-	49	014676-29-0
11	6.65	1.08	2-Octene, 2,6-dimethyl-	46	004057-42-5
12	6.769	0.69	Nonane, 3-methyl-	58	005911-04-6
13	6.961	1.65	Mesitylene	95	000108-67-8
14	7.169	1.82	1-Decene	97	000872-05-9
15	7.314	0.36	Cyclohexane, 1,1,2-trimethyl-	55	007094-26-0
16	7.496	2.75	Decane	91	000124-18-5
17	7.625	0.57	Benzene, 1,2,3-trimethyl-	95	000526-73-8
18	7.745	0.40	Octane, 1,1'-oxybis-	50	000629-82-3
19	7.833	0.40	Cyclohexane, 1-methyl-4-(1-methylethylidene)-	60	001124-27-2
20	8.009	0.60	Decane, 4-methyl-	81	002847-72-5
21	8.129	0.27	Cyclopentane, pentyl-	25	003741-00-2
22	8.248	0.30	Citronellal	42	000106-23-0
23	8.419	0.21	trans-2-Decen-1-ol, trifluoroacetate	53	1000352-67-0
24	8.502	0.38	Benzene, 4-ethyl-1,2-dimethyl-	90	000934-80-5
25	8.99	1.14	o-Cymene	91	000527-84-4
26	9.135	1.05	o-Cymene	80	000527-84-4
27	9.27	0.37	Bicyclo[3.1.1]heptan-3-one, 2,6,6-trimethyl-, (1.alpha.,2.beta.,5.alpha.)-	52	015358-88-0
28	9.416	0.30	Cyclopropane, 1-butyl-1-methyl-2-propyl-	70	041977-34-8
29	9.592	2.42	5-Undecene	93	004941-53-1
30	9.716	0.49	4-Decene, 2-methyl-, (Z)-	53	055499-07-5
31	9.929	3.64	Undecane	93	001120-21-4
32	10.37	0.39	3a,6-Methano-3aH-indene, 2,3,6,7-tetrahydro-	62	098640-29-0

33	10.583	1.29	Benzene, 2-ethenyl-1,4-dimethyl-	92	002039-89-6
34	10.739	2.09	Benzene, 1,2,4,5-tetramethyl-	95	000095-93-2
35	10.967	0.26	Benzene, 1-methyl-4-(1-methylpropyl)-	83	001595-16-0
36	11.107	0.45	Spiro[4.4]nona-1,3-diene, 1,2-dimethyl-	50	1000163-57-6
37	11.211	0.33	5-Ethyldecane	68	017302-36-2
38	11.315	0.56	Undecane, 4-methyl-	76	002980-69-0
39	11.424	0.64	Undecane, 2-methyl-	81	007045-71-8
40	11.569	1.53	2-Butene, 3-chloro-1-phenyl-, (Z)-	74	016608-68-7
41	11.761	0.95	1H-Indene, 2,3-dihydro-1,2-dimethyl-	89	017057-82-8
42	11.87	0.30	Benzene, pentamethyl-	64	000700-12-9
43	12.015	1.69	1-Undecanol	91	000112-42-5
44	12.103	0.76	4-Octene, 2,3,6,7-tetramethyl-	55	063830-66-0
45	12.332	4.03	Dodecane	94	000112-40-3
46	12.529	0.44	5-Dodecene, (E)-	92	007206-16-8
47	12.648	1.33	Undecane, 2,6-dimethyl-	93	017301-23-4
48	12.793	0.62	Benzene, 1-(2-butenyl)-2,3-dimethyl-	38	054340-85-1
49	13.006	0.34	1H-Indene, 2,3-dihydro-4,7-dimethyl-	95	006682-71-9
50	13.297	0.88	Benzene, (1-methyl-1-butenyl)-	86	053172-84-2
51	13.556	0.56	Undecane, 2,4-dimethyl-	49	017312-80-0
52	13.67	0.68	Dodecane, 2-methyl-	38	001560-97-0
53	13.769	0.22	Dodecane, 2-methyl-	83	001560-97-0
54	13.914	0.45	Tridecane, 3-methyl-	68	006418-41-3
55	14.008	0.38	Sulfurous acid, 2-ethylhexyl tridecyl ester	64	1000309-19-6
56	14.116	1.93	2-Isopropenyl-3,6-dimethylpyrazine	72	1000109-60-7
57	14.215	0.42	1H-Indene, 2,3-dihydro-1,4,7-trimethyl-	42	054340-87-3
58	14.334	1.26	1-Tridecene	98	002437-56-1
59	14.417	0.66	Cyclohexane, 2-butyl-1,1,3-trimethyl-	90	054676-39-0
60	14.641	3.92	Tridecane	97	000629-50-5
61	14.713	0.30	1.alpha.,2.beta.,3.alpha.,4.beta.-Tetramethylcyclopentane	52	002532-67-4
62	14.827	0.81	1-Tetradecene	95	001120-36-1
63	15.004	0.63	Sulfurous acid, butyl tridecyl ester	80	1000309-18-0
64	15.159	0.40	Methyl trans-4-methylcinnamate	15	020754-20-5
65	15.351	0.18	p-Menth-8(10)-en-9-ol, cis-	42	015714-13-3
66	15.766	0.84	Hexyl octyl ether	58	017071-54-4
67	15.891	0.77	Tridecane, 4-methyl-	46	026730-12-1
68	16.01	0.81	Tridecane, 2-methyl-	42	001560-96-9
69	16.14	0.35	Sulfurous acid, butyl tetradecyl ester	62	1000309-18-1
70	16.306	1.81	Dodecane, 2,6,11-trimethyl-	64	031295-56-4
71	16.451	1.68	Benzo[b]thiophene, 3,5-dimethyl-	97	001964-45-0
72	16.524	0.87	2-Tetradecene, (E)-	98	035953-54-9
73	16.617	0.34	Naphthalene, 2,7-dimethyl-	87	000582-16-1
74	16.82	3.54	Tetradecane	97	000629-59-4
75	16.887	0.28	Tridecane, 4,8-dimethyl-	96	055030-62-1
76	16.996	1.01	Dodecane, 1-fluoro-	60	000334-68-9
77	17.307	0.30	Carotol	45	000465-28-1
78	17.448	0.39	Carotol	45	000465-28-1
79	17.691	0.37	Cyclotetradecane	94	000295-17-0
80	17.8	0.50	Carbonic acid, hexadecyl prop-1-en-2-yl ester	43	1000382-90-3
81	17.987	0.27	Tetradecane, 4-methyl-	87	025117-24-2

82	18.112	1.29	Decane, 3,6-dimethyl-	55	017312-53-7
83	18.226	0.53	Tetradecane, 3-methyl-	91	018435-22-8
84	18.433	1.70	Benzo[b]thiophene, 2-ethyl-7-methyl-	87	016587-43-2
85	18.594	0.21	1-Pentadecene	99	013360-61-7
86	18.682	1.06	Benzo[b]thiophene, 2,5,7-trimethyl-	76	016587-65-8
87	18.869	3.02	Pentadecane	96	000629-62-9
88	19.02	0.46	Benzene, ethylpentamethyl-	68	002388-04-7
89	19.367	0.31	(+)-2-Carene, 2-isopropenyl-	51	1000151-27-0
90	19.544	0.58	2,2'-Ethylidenebis(5-methylfuran)	60	003209-79-8
91	19.746	0.58	Cyclopentadecane	93	000295-48-7
92	19.845	0.42	4,5,6,7-Tetramethylphthalide	43	029002-54-8
93	19.959	0.64	Benzo[b]thiophene, 2,7-diethyl-	70	016587-45-4
94	20.057	0.35	Decane, 3,8-dimethyl-	90	017312-55-9
95	20.192	0.65	Decane, 3,8-dimethyl-	74	017312-55-9
96	20.53	0.41	2-Tetradecene, (E)-	91	035953-54-9
97	20.628	0.35	1-Decanol, 2-hexyl-	96	002425-77-6
98	20.794	2.45	Hexadecane	97	000544-76-3
99	21.723	0.63	Tritetracontane	72	007098-21-7
100	21.931	0.66	Carbonic acid, hexadecyl prop-1-en-2-yl ester	46	1000382-90-3
101	22.065	0.41	Tetradecane, 2,6,10-trimethyl-	89	014905-56-7
102	22.398	0.35	1-Octadecene	99	000112-88-9
103	22.621	1.91	Heptadecane	98	000629-78-7
104	22.756	0.32	Pentadecane, 2,6,10-trimethyl-	81	003892-00-0
105	23.549	0.29	Heptadecyl heptafluorobutyrate	90	959085-66-6
106	24.156	0.20	1-Octadecene	99	000112-88-9
107	24.364	1.32	Octadecane	98	000593-45-3
108	24.561	0.30	Hexadecane, 2,6,10,14-tetramethyl-	95	000638-36-8
109	25.308	0.19	Hexadecane	83	000544-76-3
110	26.024	1.02	Heneicosane	96	000629-94-7
111	27.021	0.25	Ethanol, 2-(octadecyloxy)-	90	002136-72-3
112	27.607	0.73	Eicosane	98	000112-95-8
113	29.127	0.53	Heneicosane	98	000629-94-7
114	30.585	0.36	Heptadecane	95	000629-78-7
115	31.981	0.24	Tetracosane	97	000646-31-1
116	33.325	0.18	Tetracosane	98	000646-31-1
117	37.325	1.16	1,4-Benzenedicarboxylic acid, bis(2-ethylhexyl) ester	91	006422-86-2
118	37.777	0.21	Hexanedioic acid, bis[2-(2-butoxyethoxy)ethyl] ester	50	000141-17-3

Table8: The compounds identified through Gas Chromatography-Mass Spectrometry (GC-MS) analysis of used G2**.**

No	RT (min)	Area%	Name	Quality	CAS Number
1	4.211	0.28	Cyclopropane, pentyl-	52	002511-91-3
2	4.378	0.80	p-Xylene	83	000106-42-3
3	4.507	0.42	Octane, 4-methyl-	49	002216-34-4
4	4.652	0.69	Octane, 3-methyl-	58	002216-33-3
5	4.964	1.09	1-Nonene	81	000124-11-8
6	5.213	1.51	Nonane	91	000111-84-2

7	6.38	0.29	trans-3-Decene	64	019150-21-1
8	6.619	0.65	Heptane, 2,3,4-trimethyl-	47	052896-95-4
9	6.764	0.39	Heptane, 5-ethyl-2,2,3-trimethyl-	50	062199-06-8
10	6.956	0.20	Mesitylene	95	000108-67-8
11	7.164	0.99	1-Decene	96	000872-05-9
12	7.309	0.24	Cyclohexane, 1,2,3-trimethyl-, (1.alpha.,2.beta.,3.alpha.)-	64	001678-81-5
13	7.475	1.76	Decane	91	000124-18-5
14	7.61	0.35	Mesitylene	95	000108-67-8
15	7.74	0.25	Heptane, 3,3-dimethyl-	38	004032-86-4
16	7.833	0.23	Benzene, 2-propenyl-	53	000300-57-2
17	8.004	0.38	Decane, 4-methyl-	90	002847-72-5
18	8.238	0.24	Cyclopentane, hexyl-	60	004457-00-5
19	8.497	0.24	cis-3-Decene	49	019398-86-8
20	8.684	0.23	Benzene, 1-methyl-4-propyl-	35	001074-55-1
21	8.98	0.30	o-Cymene	91	000527-84-4
22	9.13	0.67	Benzene, 4-ethyl-1,2-dimethyl-	60	000934-80-5
23	9.26	0.27	8-Oxabicyclo[5.1.0]oct-5-en-2-ol, 1,4,4-trimethyl-	50	058795-43-0
24	9.416	0.37	1-Nonene	70	000124-11-8
25	9.587	1.73	Cyclopropane, 1-heptyl-2-methyl-	91	074663-91-5
26	9.909	2.39	Undecane	90	001120-21-4
27	10.578	0.79	Benzene, 2-ethenyl-1,4-dimethyl-	92	002039-89-6
28	10.734	1.75	Benzene, 1,2,4,5-tetramethyl-	95	000095-93-2
29	10.894	0.27	2-Acetonylcyclohexanone	42	006126-53-0
30	11.107	0.22	Cyclopentane, 1-methyl-2-(4-methylpentyl)-, trans-	25	066553-50-2
31	11.304	0.47	Undecane, 4-methyl-	76	002980-69-0
32	11.413	0.43	Undecane, 2-methyl-	64	007045-71-8
33	11.559	1.03	2-Butene, 3-chloro-1-phenyl-, (Z)-	74	016608-68-7
34	11.751	0.48	1H-Indene, 2,3-dihydro-1,2-dimethyl-	83	017057-82-8
35	11.834	0.30	2-Undecene, 10-methyl-	46	1000061-83-3
36	12.01	1.32	2-Dodecene, (E)-	93	007206-13-5
37	12.093	0.32	Cyclopentane, (2-methylpropyl)-	45	003788-32-7
38	12.311	2.79	Dodecane	95	000112-40-3
39	12.518	0.26	Cyclododecane	64	000294-62-2
40	12.633	1.00	Undecane, 2,6-dimethyl-	93	017301-23-4
41	12.778	0.40	1H-Indene, 2,3-dihydro-1,1,3-trimethyl-	72	002613-76-5
42	13.292	0.61	Benzene, 1-methyl-3-(1-methyl-2-propenyl)-	41	052161-57-6
43	13.51	0.64	Decyl octyl ether	58	1000406-38-3
44	13.66	0.50	Dodecane, 2-methyl-	42	001560-97-0
45	13.904	0.58	1-Iodo-2-methylundecane	72	073105-67-6
46	13.997	0.23	Sulfurous acid, 2-ethylhexyl heptadecyl ester	49	1000309-20-0
47	14.117	1.22	Benzo[b]thiophene, 2-methyl-	87	001195-14-8
48	14.21	0.21	Benzene, 1-(2-butenyl)-2,3-dimethyl-	35	054340-85-1
49	14.335	1.22	1-Tridecene	98	002437-56-1
50	14.433	0.64	3-Tetradecene, (E)-	93	041446-68-8
51	14.625	2.88	Tridecane	95	000629-50-5
52	14.999	0.44	Carbonic acid, prop-1-en-2-yl tridecyl ester	80	1000382-90-8

53	15.16	0.25	Benzaldehyde, 4-methyl-	25	000104-87-0
54	15.761	0.71	Carbonic acid, decyl undecyl ester	30	1000383-16-0
55	15.896	0.60	Dodecane, 4-methyl-	38	006117-97-1
56	16.016	0.54	Benzene, 1,3,5-triethyl-	64	000102-25-0
57	16.145	0.24	3,5-Dimethyldodecane	60	107770-99-0
58	16.27	0.27	2,5-Dimethylthiophene-3,4-dicarbonitrile	83	1000305-40-9
59	16.467	0.89	Benzo[b]thiophene, 3,5-dimethyl-	97	001964-45-0
60	16.545	0.91	2-Tetradecene, (E)-	98	035953-54-9
61	16.825	3.04	Tetradecane	96	000629-59-4
62	16.898	0.21	Decane, 3,8-dimethyl-	55	017312-55-9
63	17.012	0.50	Pentadecafluorooctanoic acid, tetradecyl ester	43	1000406-04-4
64	17.458	0.42	4,4-Dimethyladamantan-2-ol	56	1000210-61-2
65	17.707	0.32	Cyclotetradecane	93	000295-17-0
66	17.795	0.48	Carbonic acid, dodecyl vinyl ester	46	1000382-54-8
67	17.93	0.37	1-Decanol, 2-hexyl-	50	002425-77-6
68	18.013	0.43	Tetradecane, 4-methyl-	80	025117-24-2
69	18.133	0.39	Decane, 3,6-dimethyl-	60	017312-53-7
70	18.252	0.28	Tetradecane, 3-methyl-	89	018435-22-8
71	18.475	3.00	Benzo[b]thiophene, 2-ethyl-5-methyl-	91	016587-51-2
72	18.641	0.52	2-Tetradecene, (E)-	97	035953-54-9
73	18.719	1.29	2,4-Pentanedione, 3-phenyl-	64	005910-25-8
74	18.895	2.59	Pentadecane	96	000629-62-9
75	19.061	0.63	Benzo[b]thiophene, 2,5,7-trimethyl-	76	016587-65-8
76	19.264	0.23	Naphthalene, 2,3,6-trimethyl-	66	000829-26-5
77	19.404	0.44	1,4-Cyclohexadiene, 6-isopropenyl-1,2,3,4-tetramethyl-	70	1000160-89-3
78	19.58	0.79	Benzo[b]thiophene, 2,7-diethyl-	70	016587-45-4
79	19.798	0.34	Cyclopentadecane	90	000295-48-7
80	19.892	0.57	4,5,6,7-Tetramethylphthalide	49	029002-54-8
81	20.011	1.07	Benzo[b]thiophene, 2,7-diethyl-	89	016587-45-4
82	20.104	0.27	Pentadecane, 2-methyl-	66	001560-93-6
83	20.234	0.58	Pentadecane, 3-methyl-	68	002882-96-4
84	20.333	0.24	Benzo[b]thiophene, 2,3-diethyl-	90	054789-20-7
85	20.436	0.35	Benzene, 1-ethyl-3,5-diisopropyl-	64	015181-13-2
86	20.587	0.90	Cetene	93	000629-73-2
87	20.685	0.38	Benzo[b]thiophene, 2,3-diethyl-	70	054789-20-7
88	20.851	2.55	Hexadecane	97	000544-76-3
89	21.505	0.28	Benzo[b]thiophene, 2-ethyl-5,7-dimethyl-	70	018428-05-2
90	21.671	0.31	Tetradecane, 1-chloro-	42	002425-54-9
91	21.791	0.73	Decane, 3,6-dimethyl-	83	017312-53-7
92	21.998	1.12	Hexadecane, 2-methyl-	56	001560-92-5
93	22.128	0.56	Tetradecane, 1-chloro-	62	002425-54-9
94	22.361	0.26	4-(2,6,6-Trimethyl-cyclohexa-1,3-dienyl)-pent-3-en-2-one	66	1000192-39-9
95	22.47	0.65	3-Heptadecene, (Z)-	97	1000141-67-3
96	22.704	2.28	Heptadecane	96	000629-78-7
97	22.828	0.24	Heptadecane, 3-methyl-	78	006418-44-6
98	23.181	0.26	Cyclotetradecane	60	000295-17-0
99	23.908	0.67	Heptadecane, 3-methyl-	95	006418-44-6
100	24.245	0.63	1-Octadecene	99	000112-88-9

101	24.463	2.04	Octadecane	97	000593-45-3
102	25.023	0.45	1-Methyldibenzothiophene	91	031317-07-4
103	25.142	0.34	Hexadecane, 1-chloro-	50	004860-03-1
104	25.386	0.57	2-Methyldibenzothiophene	72	1000383-55-1
105	25.49	0.30	Anthracene, 1-methyl-	89	000610-48-0
106	25.62	0.29	Octadecane, 3-methyl-	90	006561-44-0
107	25.926	0.30	1-Octadecene	99	000112-88-9
108	26.139	1.71	Nonadecane	97	000629-92-5
109	26.408	0.41	Dibenzothiophene, 4,6-dimethyl-	98	001207-12-1
110	26.761	0.66	3,7-Dimethyldibenzothiophene	98	001136-85-2
111	27.125	1.15	3,7-Dimethyldibenzothiophene	96	001136-85-2
112	27.737	1.62	Eicosane	99	000112-95-8
113	27.841	0.33	Phenanthrene, 3,6-dimethyl-	60	001576-67-6
114	28.302	0.26	4'-Methoxy-2-hydroxystilbene	55	1000147-93-1
115	28.432	0.29	(Acridin-9-yl)(methyl)amine	30	1000305-13-9
116	28.583	0.34	Benzenamine, 4,4'-methylenebis[2-methyl-	64	000838-88-0
117	28.676	0.21	1-Octadecene	91	000112-88-9
118	28.754	0.36	Anthracene, 1,8-diethynyl-	86	078053-58-4
119	28.941	0.36	5(10H)-Pyrido[3,4-b]quinolone, 7-methoxy-	83	1000256-99-5
120	29.252	1.78	Heneicosane	98	000629-94-7
121	29.797	0.20	Hexadecane	95	000544-76-3
122	29.973	0.38	[2,2'-Bithiophene]-5,5'-dicarboxaldehyde	64	1000327-35-6
123	30.71	1.23	Heptadecane	98	000629-78-7
124	31.249	0.20	1-Chloroeicosane	95	042217-02-7
125	32.106	1.25	Octadecane	96	000593-45-3
126	33.449	0.97	Tetracosane	98	000646-31-1
127	33.942	0.36	5-Methylbenzo[b]naphtho[2,1-d]thiophene	91	004567-49-1
128	34.233	0.32	3-Methylphenanthro[9,10-b]thiophene	89	082420-70-0
129	34.601	0.29	2,6,10,14-Tetramethyl-7-(3-methylpent-4-enylidene) pentadecane	93	1000370-41-6
130	34.736	0.88	Octadecane	97	000593-45-3
131	35.157	0.29	1-Chloroeicosane	95	042217-02-7
132	35.976	0.75	Triacontane	98	000638-68-6
133	36.189	0.21	1-Hexacosene	93	018835-33-1
134	36.376	0.23	Docosane	93	000629-97-0
135	36.718	0.20	Eicosane	95	000112-95-8
136	37.17	0.55	Eicosane	98	000112-95-8
137	37.398	0.48	1,4-Benzenedicarboxylic acid, bis(2-ethylhexyl) ester	91	006422-86-2
138	38.322	0.47	Octacosane	98	000630-02-4
139	39.437	0.50	Heptacosane, 1-chloro-	98	062016-79-9
140	40.516	0.40	Triacontane	98	000638-68-6
141	41.684	0.33	Heptacosane, 1-chloro-	99	062016-79-9
142	43.028	0.29	Heptacosane, 1-chloro-	98	062016-79-9
143	44.6	0.21	Tritriacontane	98	000630-05-7
144	46.478	0.26	Nonacosane	99	000630-03-5
145	48.72	0.22	Tritriacontane	97	000630-05-7

Table 9: The compounds identified through Gas Chromatography-Mass Spectrometry (GC-MS) analysis of used G2***.**

No	RT (min)	Area%	Name	Quality	CAS Number
1	3.175	2.46	Octane	86	000111-65-9
2	4.022	1.63	1-Nonene	93	000124-11-8
3	4.138	3.01	Nonane	91	000111-84-2
4	4.794	3.05	Heptane, 2,3,4-trimethyl-	53	052896-95-4
5	5.206	2.55	Decane	94	000124-18-5
6	5.334	1.59	Benzene, 1,2,4-trimethyl-	90	000095-63-6
7	5.74	1.32	Benzene, 1-ethyl-3,5-dimethyl-	89	000934-74-7
8	5.891	1.54	Methoxyacetic acid, 2-ethylhexyl ester	72	1000282-41-4
9	6.007	2.14	Decane, 3-methyl-	94	013151-34-3
10	6.216	2.31	1-Undecene	91	000821-95-4
11	6.349	4.07	Undecane	95	001120-21-4
12	6.802	1.77	1H-Indene, 2,3-dihydro-4-methyl-	93	000824-22-6
13	6.854	2.35	Benzene, 1-ethyl-3,5-dimethyl-	95	000934-74-7
14	7.417	3.87	Cyclododecane	93	000294-62-2
15	7.557	5.36	Dodecane	97	000112-40-3
16	7.748	3.03	Undecane, 2,6-dimethyl-	93	017301-23-4
17	8.067	1.50	1-Tridecene	80	002437-56-1
18	8.212	2.59	Oxalic acid, decyl 2-ethylhexyl ester	43	1000309-39-3
19	8.433	1.75	1H-Indene, 2,3-dihydro-1,2-dimethyl-	35	017057-82-8
20	8.665	6.52	1-Tridecene	95	002437-56-1
21	8.799	5.36	Tridecane	97	000629-50-5
22	8.938	1.26	Cyclotetradecane	94	000295-17-0
23	9.762	1.46	Dodecane, 2,6,11-trimethyl-	86	031295-56-4
24	9.89	2.87	3-Tetradecene, (E)-	97	041446-68-8
25	9.971	2.01	Benzo[b]thiophene, 3,5-dimethyl-	94	001964-45-0
26	10.029	5.14	Tetradecane	96	000629-59-4
27	10.609	1.24	Cyclotetradecane	97	000295-17-0
28	10.807	1.22	Hexacosane	74	000630-01-3
29	11.103	3.67	2-Acetyl-7-hydroxybenzofuran	58	040020-87-9
30	11.23	3.47	Pentadecane	97	000629-62-9
31	11.776	1.67	Ethanol, 2-(dodecyloxy)-	48	004536-30-5
32	12.385	2.83	Hexadecane	98	000544-76-3
33	13.494	2.42	Heptadecane	97	000629-78-7
34	14.55	2.13	Octadecane	98	000593-45-3
35	15.56	1.55	Nonadecane	98	000629-92-5
36	16.529	1.13	Eicosane	97	000112-95-8
37	17.452	0.87	Heneicosane	99	000629-94-7
38	18.34	0.84	Heptadecane	95	000629-78-7
39	19.188	0.57	Tetracosane	99	000646-31-1
40	20.006	0.53	Tetracosane	99	000646-31-1
41	22.461	3.37	1,4-Benzenedicarboxylic acid, bis(2-ethylhexyl) ester	91	006422-86-2

5. Conclusions

Kaolin-based geopolymers were evaluated as heterogeneous catalysts for cracking Iraqi vacuum residual. The primary aim of this research was to synthesize an economically feasible and environmentally friendly geopolymer catalyst from kaolin and increase activity by ion exchange use HCl leaching, investigate its properties, and assess its effectiveness in vacuum residual cracking. Initially, conventional geopolymers were prepared using two types of kaolin, classified based on iron content (red and white). Subsequently, conventional geopolymers were treated with HCl to enhance catalyst activity in a fixed-bed reactor at temperatures ranging from 410°C, with a reaction time of 15-30 minutes.

Researchers developed several geopolymer catalysts and tested them for cracking heavy oil into useful products. They found that catalysts with more iron were better at making gasoline and kerosene, while those with less iron were better at removing sulfur. In summary, the novel results from Gas Chromatography-Mass Spectrometry (GC-MS) confirmed that geopolymers serve as friendly and inexpensive cracking catalysts. Overall, the study suggests geopolymers are promising as cracking catalysts, and further optimization could lead to even more efficient and targeted fuel production.

References:

[1] C. Cheeseman and A. R. Boccaccini, "Metakaolin based geopolymers to encapsulate nuclear waste PhD thesis," 2013.

[2] J. Kwasny, W. Sha, and M. Soutsos, "Effect of slag content and activator dosage on the resistance of fly ash geopolymer binders to sulfuric acid attack," no. May 2019, 2018, doi: 10.1016/j.cemconres.2018.06.011.

[3] P. Cong and Y. Cheng, "Advances in geopolymer materials: A comprehensive review," *J. Traffic Transp. Eng. (English Ed.*, vol. 8, no. 3, pp. 283–314, 2021, doi: 10.1016/j.jtte.2021.03.004.

[4] G. Samson *et al.*, "Formulation and characterization of blended alkali-activated materials based on flash-calcined metakaolin , fly ash and GGBS To cite this version : HAL Id : hal-01756694," 2018, doi: 10.1016/j.conbuildmat.2017.03.160.Highlights.

[5] C. Republic and C. Republic, "MICROSTRUCTURE OF GEOPOLYMER MATERIALS BASED ON FLY ASH," vol. 50, no. 4, pp. 208–215, 2006.

[6] J. Davidovits and S. France, "Geopolymer chemistry and sustainable development Geopolymer chem istry and sustain able Dev elopment . The Poly (s ialate) term inolog y : a v ery useful and simp le model for th e p rom otion and understanding of green-chemistr y .," no. July 2005, 2018.

[7] J. Davidovits and S. France, "Geopolymers: Man-made rock geosynthesis and the resulting development of very early high strength cement," no. November, 2018.

[8] K. Tan and E. Yang, "A critical review of geopolymer properties for structural fire-resistance applications," no. October, 2019, doi: 10.1016/j.conbuildmat.2019.06.076.

[9] R. M. Novais, R. C. Pullar, and J. A. Labrincha, "Geopolymer foams: an overview of recent

advancements," *Prog. Mater. Sci.*, p. 100621, 2019, doi: 10.1016/j.pmatsci.2019.100621.

[10] H. Alshabebi, "The Legal Framework of The Oil and Gas Industry In Iraq," *Akkad J. Law Public Policy*, vol. 1, no. 2, pp. 44–53, 2022, doi: 10.55202/ajlpp.v1i2.66.

[11] P. Taylor, "' The Demetallization of Residual Fuel Oil and Petroleum Residue This article was downloaded by : [Maier , Ludwig] Access details : Access Details : [subscription number 927263716] Petroleum Science and Technology," no. May, 2014, doi: 10.1080/10916460903226122.

[12] M. H. Ismael and N. A. Igorevich, "Study of hydrocarbon composition petroleum fractions and evaluation of crude oil at Iraq (east Iraq) and produce diesel fuel," vol. 7, no. 1, pp. 1065–1071, 2022.

[13] S. Sotirov, E. Sotirova, and D. D. Stratiev, "Effect of Crude Oil Quality on Properties of Hydrocracked Vacuum Residue and Its Blends with Cutter Stocks to Produce Fuel Oil," 2023.

[14] R. Sahu, B. J. Song, J. S. Im, Y. P. Jeon, and C. W. Lee, "A review of recent advances in catalytic hydrocracking of heavy residues," *J. Ind. Eng. Chem.*, vol. 27, pp. 12–24, 2015, doi: 10.1016/j.jiec.2015.01.011.

[15] R. Sahu, B. Jin, J. Sun, Y. Jeon, and C. Wee, "Journal of Industrial and Engineering Chemistry A review of recent advances in catalytic hydrocracking of heavy residues," *J. Ind. Eng. Chem.*, vol. 27, pp. 12–24, 2015, doi: 10.1016/j.jiec.2015.01.011.

[16] I. O. P. C. Series and M. Science, "Effect of Iron Oxide (Fe 2 O 3) on the Properties of Fly Ash Based Effect of Iron Oxide (Fe 2 O 3) on the Properties of Fly Ash Based Geopolymer," 2020, doi: 10.1088/1757-899X/877/1/012017.

[17] R. K. Gupta and P. Gera, "PROCESS FOR THE UPGRADATION OF PETROLEUM RESIDUE : REVIEW," no. 03, pp. 643–656, 2015.

[18] S. M. Sadrameli, "Thermal/catalytic cracking of liquid hydrocarbons for the production of olefins: A state-of-the-art review II: Catalytic cracking review," *Fuel*, vol. 173, no. January, pp. 285–297, 2016, doi: 10.1016/j.fuel.2016.01.047.

[19] S. Haridoss, "A Study on Role of Catalyst used in Catalytic Cracking process in Petroleum Refining," vol. 10, no. 7, pp. 79–86, 2017.

[20] S. M. Refinery, E. S. Projects, C. Confidential, and B. Information, "General Process Description of a Catalytic Cracking Unit," no. 1, pp. 1–27, 2018.

[21] K. S. AlKhafaji, B. Y. Al-Zaidi, Z. M. Shakor, and S. J. Hussein, "Comparison between Conventional and Metakaolin bi-functional Catalyst in the Hydrodesulfurization Operation," *J. Pet. Res. Stud.*, vol. 12, no. 2, pp. 64–80, 2022, doi: 10.52716/jprs.v12i2.658.

[22] L. Vieira, L. J. Maschio, E. P. De Araújo, A. M. Da Silva, and R. Vieira, "Development of geopolymers for catalyst support applications," *Mater. Res.*, vol. 22, no. 6, 2019, doi: 10.1590/1980-5373-MR-2018-0770.

[23] F. Moodi, A. A. Ramezanianpour, and A. S. Safavizadeh, "Evaluation of the optimal process of thermal activation of kaolins," *Sci. Iran.*, vol. 18, no. 4 A, pp. 906–912, 2011, doi: 10.1016/j.scient.2011.07.011.

[24] E. Mohseni, "Assessment of Na2SiO3 to NaOH ratio impact on the performance of polypropylene fiber-reinforced geopolymer composites," *Constr. Build. Mater.*, vol. 186, pp. 904–911, 2018, doi: 10.1016/j.conbuildmat.2018.08.032.

[25] L. Han *et al.*, "Synthesis of fly ash-based self-supported zeolites foam geopolymer via saturated steam treatment," *J. Hazard. Mater.*, vol. 393, no. January, p. 122468, 2020, doi: 10.1016/j.jhazmat.2020.122468.

[26] J. D. 2008, *Geopolymer CHemistry and Applications, 5th edition*, no. January 2008. 2008. [Online]. Available: https://www.researchgate.net/publication/265076752

[27] P. K. Seelam *et al.*, "Modified geopolymers as promising catalyst supports for abatement of dichloromethane," *J. Clean. Prod.*, vol. 280, no. xxxx, 2021, doi: 10.1016/j.jclepro.2020.124584.

[28] E. Kränzlein, J. Harmel, H. Pöllmann, and W. Krcmar, "Influence of the Si / Al ratio in geopolymers on the stability against acidic attack and the immobilization of Pb 2 + and Zn 2 +," *Constr. Build. Mater.*, vol. 227, p. 116634, 2019, doi: 10.1016/j.conbuildmat.2019.08.015.

[29] J. W. Phair and J. S. J. Van Deventer, "Effect of the silicate pH on the microstructural characteristics of waste-based geopolymers," *Int. J. Miner. Process.*, vol. 66, no. 1–4, pp. 121–143, 2002, doi: 10.1016/S0301-7516(02)00013-3.

[30] F. Rizal, A. P. Pratama, Khamistan, A. Fauzi, Syarwan, and A. Azka, "Effect of H2O2 as the Foaming Agent on the Geopolymer Mortar using Curing of Room Temperature," *IOP Conf. Ser. Mater. Sci. Eng.*, vol. 854, no. 1, 2020, doi: 10.1088/1757-899X/854/1/012022.

[31] P. Duxson, S. W. Mallicoat, G. C. Lukey, W. M. Kriven, and J. S. J. van Deventer, "The effect of alkali and Si/Al ratio on the development of mechanical properties of metakaolin-based geopolymers," *Colloids Surfaces A Physicochem. Eng. Asp.*, vol. 292, no. 1, pp. 8–20, 2007, doi: 10.1016/j.colsurfa.2006.05.044.

[32] M. I. M. Alzeer, K. J. D. MacKenzie, and R. A. Keyzers, "Porous aluminosilicate inorganic polymers (geopolymers): a new class of environmentally benign heterogeneous solid acid catalysts," *Appl. Catal. A Gen.*, vol. 524, pp. 173–181, 2016, doi: 10.1016/j.apcata.2016.06.024.

[33] M. Urbanova, L. Kobera, and J. Brus, "Factor analysis of 27 Al MAS NMR spectra for identifying nanocrystalline phases in amorphous geopolymers," no. June, pp. 734–742, 2013, doi: 10.1002/mrc.4009.

[34] B. Zhang, Æ. K. J. D. Mackenzie, and I. W. M. Brown, "Phase Development of NaOH Activated Blast Furnace Slag Geopolymers Cured Crystalline phase formation in metakaolinite geopolymers activated with NaOH and sodium silicate," no. November 2016, 2009, doi: 10.1063/1.3203243.

[35] A. Saeed *et al.*, "Properties and Applications of Geopolymer Composites : A Review Study of Mechanical and Microstructural Properties," 2022.

[36] V. Mathivet *et al.*, "Acid-based geopolymers : Understanding of the structural evolutions during consolidation and after thermal treatments," *J. Non. Cryst. Solids*, vol. 512, no. February, pp. 90–97, 2019, doi: 10.1016/j.jnoncrysol.2019.02.025.

[37] A. Autef, E. Joussein, G. Gasgnier, and S. Rossignol, "Role of the silica source on the geopolymerization

rate," *J. Non. Cryst. Solids*, vol. 358, no. 21, pp. 2886–2893, 2012, doi: 10.1016/j.jnoncrysol.2012.07.015.

[38] A. Hajimohammadi and J. S. J. Deventer, "Characterisation of One-Part Geopolymer Binders Made from Fly," *Waste and Biomass Valorization*, vol. 8, no. 1, pp. 225–233, 2017, doi: 10.1007/s12649-016-9582-5.

[39] M.-I. Khan, K. Azizli, S. Sufian, A. A. Siyal, and Z. Man, "Sodium Silicate Free Geopolymer As Coating Material : Adhesion To Steel Sodium Silicate Free Geopolymer As Coating Material : Adhesion To Steel," no. November, 2014, doi: 10.3390/ecm-1-b016.

[40] F. J. H. Tommasini Vieira Ramos, M. de Fátima Marques Vieira, L. G. P. Tienne, and V. de Oliveira Aguiar, "Evaluation and characterization of geopolymer foams synthesized from blast furnace with sodium metasilicate," *J. Mater. Res. Technol.*, vol. 9, no. 5, pp. 12019–12029, 2020, doi: 10.1016/j.jmrt.2020.08.019.

[41] R. O. Ajemba and O. D. Onukwuli, "Studies of the Effects Of Hydrochloric Acid-Leaching On The Structural And Adsorptive Performance Of NTEJE (Nigeria) Clay," vol. 1, no. 3, pp. 1–11, 2012.

[42] C. Chizallet and P. Raybaud, "Pseudo-Bridging Silanols as Versatile Brønsted Acid Sites of Amorphous Aluminosilicate Surfaces **," vol. 3, no. 100, pp. 2891–2893, 2009, doi: 10.1002/anie.200804580.

[43] T. Li *et al.*, "Synthesis and characterization of amorphous silica-alumina with enhanced acidity and its application in hydro-isomerization / cracking," *Fuel*, vol. 279, no. June, p. 118487, 2020, doi: 10.1016/j.fuel.2020.118487.

[44] W. Wu and E. Weitz, "Modification of Acid Sites in ZSM-5 by Ion-exchange: An in-situ FTIR Study," *Appl. Surf. Sci.*, 2014, doi: 10.1016/j.apsusc.2014.07.194.

[45] M. Tamura, K. Shimizu, and A. Satsuma, "Applied Catalysis A : General Comprehensive IR study on acid / base properties of metal oxides," *"Applied Catal. A, Gen.*, vol. 433–434, pp. 135–145, 2012, doi: 10.1016/j.apcata.2012.05.008.

[46] G. S. Foo, D. Wei, D. S. Sholl, and C. Sievers, "378799 Role of Lewis and Brnsted Acid Sites in the Dehydration of Glycerol over Niobia Role of Lewis and Brønsted Acid Sites in the Dehydration of Glycerol over Niobia," no. November 2014, 2015.

[47] A. A. M. Ć and L. R. M. Č. I. Ć, "THERMAL TREATMENT OF KAOLIN CLAY TO OBTAIN METAKAOLIN," no. March, pp. 351–356, 2010, doi: 10.2298/HEMIND100322014I.

[48] M. Moliner, M. Meira, and M. Boronat, "Chemical Science Tailoring Lewis / Brønsted acid properties of MOF nodes via hydrothermal and solvothermal synthesis : simple approach with exceptional catalytic implications †," pp. 10106–10115, 2021, doi: 10.1039/d1sc02833b.

[49] D. Panias, M. Taxiarchou, I. Paspaliaris, and A. Kontopoulos, "Mechanisms of dissolution of iron oxides in aqueous oxalic acid solutions," no. November 2017, 1996, doi: 10.1016/0304-386X(95)00104-O.

[50] A. Feliczak-Guzik, "Hierarchical zeolites: Synthesis and catalytic properties," *Microporous Mesoporous Mater.*, vol. 259, pp. 33–45, 2018, doi: 10.1016/j.micromeso.2017.09.030.

[51] M. I. M. Al-zeer and K. J. D. Mackenzie, "Fly Ash-Based Geopolymers as Sustainable Bifunctional Heterogeneous Catalysts and Their Reactivity in Friedel-Crafts Acylation Reactionsc," 2019.